

# Lévy imaging of elastic hadron-hadron scattering: Odderon and inner structure of the proton

T. CSÖRGŐ<sup>1,2,3</sup>, R. PASECHNIK<sup>4</sup> AND A. STER<sup>1</sup>

<sup>1</sup>MTA WIGNER FK, H-1525 Budapest 114, POB 49, Hungary

<sup>2</sup>EKU KRC, H-3200 Gyöngyös, Mátrai út 36, Hungary

<sup>3</sup>CERN, CH-1211 Geneva 23, Switzerland

<sup>4</sup>Department of Astronomy and Theoretical Physics,  
Lund University, SE-223 62 Lund, Sweden

A novel model-independent Lévy imaging method is employed for reconstruction of the elastic  $pp$  and  $p\bar{p}$  scattering amplitudes at low and high energies. The four-momentum transfer  $t$  dependent elastic slope  $B(t)$ , the nuclear phase  $\phi(t)$  as well as the excitation function of the shadow profile  $P(b)$  have been extracted from data at ISR, Tevatron and LHC energies. We found qualitative differences in properties of  $B(t)$  and  $\phi(t)$  between  $pp$  and for  $p\bar{p}$  collisions, that indicate an Odderon effect. A proton substructure has also been identified and found to have two different sizes, comparable to that of a dressed quark at the ISR and of a dressed diquark at the LHC energies, respectively.

## 1. Introduction

Recently, new data on the total, elastic and differential cross-section measurements in elastic  $pp$  collisions  $\sqrt{s} = 13$  TeV have become available from the TOTEM Collaboration at the Large Hadron Collider (LHC) [1, 2] indicating a possible effect of the C-odd three-gluon state known as Odderon [3]. These data have triggered an intense debate in the literature, see e.g. refs. [4]–[13]. Here, we contribute to this discussion with the results of our model-independent analysis of the most recent TOTEM data set at the highest currently available energy of  $\sqrt{s} = 13$  TeV [14].

## 2. Model-independent Lévy imaging method

Our imaging method is based on a recently found, model independent Levy expansion. For a detailed presentation of this novel and sophisticated imaging technique, see [13], while for a brief summary of the main results,

see [15]. In this manuscript we highlight only some of the most interesting results of this approach. This method is a straightforward generalisation of the well-known Laguerre, Edgeworth [16] and Lévy [17] expansions proposed for characterisation of the nearly Lévy stable source distributions typically used in studies of particle correlations and femtoscopy.

We proposed to apply the Lévy expansion (with complex coefficients) at the level of the elastic amplitude [13, 15], to have a positive definite expression for the differential cross-section of elastic scattering. This way, we obtained the following representation of the elastic amplitude  $T_{el}(\Delta)$

$$\frac{d\sigma}{dt} = \frac{1}{4\pi} |T_{el}(\Delta)|^2, \quad T_{el}(\Delta) = i\sqrt{4\pi Aw(z|\alpha)} \left[ 1 + \sum_{i=1}^{\infty} c_i l_i(z|\alpha) \right], \quad (1)$$

where  $\Delta = \sqrt{|t|}$ , the four-momentum transfer is denoted by  $t = (p_1 - p_3)^2 < 0$  and  $w(z|\alpha) = \exp(-z^\alpha)$  stands for the Lévy weight known also as the stretched exponential distribution,  $z = |t|R^2$  is the dimensionless positively-definite scaling variable, constructed from  $|t|$  and a Lévy scale parameter  $R$  (represented in units of fermi in what follows),  $c_j = a_j + ib_j$  are the complex coefficients of the Levy expansion, and  $l_j(z|\alpha)$  stands for the orthonormal set of Lévy polynomials. The orthonormal Lévy polynomials introduced above are detailed in ref. [13]. This Levy expansion method leads to simple expressions for the total, elastic and differential cross-sections, as well as for the  $t$  dependent nuclear slope  $B(t)$  and the ratio of the real to imaginary part of the forward scattering amplitude  $\rho(t)$  and the nuclear phase  $\phi(t)$ , as summarized briefly in ref. [15] and explained in greater detail in ref. [13].

In our approach, the stretched exponential  $w(z|\alpha)$  characterises the degree of non-exponentiality in the elastic scattering cross-section  $d\sigma/dt \propto \exp(-(R^2|t|)^\alpha)$  at small  $|t| \ll R^{-2}$  below the diffractive minimum i.e. in the diffractive cone. The non-exponentiality, even though subtle, has been confirmed by the TOTEM analysis of  $\sqrt{s} = 8$  TeV elastic  $pp$  scattering data as a more than  $7\sigma$  effect [18]. This means that in the conventional exponential parameterisation  $\frac{d\sigma}{dt} = A \exp(-B|t|)$  the diffractive slope  $B$  is expected to be a non-trivial function of  $|t|$  whose deviation from a constant is a relevant measure of non-exponentiality.

### 3. Fit results

In Fig. 1, we present an example of the quality fits we have performed for the differential elastic cross-section adopting the fourth-order Lévy expansion of the elastic amplitude (1). Generically, as a necessary condition for interpretations of such fits, we consider a statistically acceptable confidence level of  $CL > 0.1\%$ . As detailed in ref. [13], such good quality fits

were achieved for almost all of the published data sets, for both  $pp$  and  $p\bar{p}$  cases. In case of the 7 TeV  $pp$  data, we obtained a marginal confidence level of  $CL \approx 0.02\%$ , as indicated in Fig. 1 (left panel). While one may try to use this fit result for physics interpretation as well, one may need to repeat the analysis of 7 TeV  $pp$  data including the full covariance matrix, and/or to study the Lévy fits to the low- $t$  and the large- $t$  part of the 7 TeV dataset separately. Another possibility is to add the statistical and systematic errors in quadrature at 7 TeV, similarly to our analysis of the 13 TeV data.

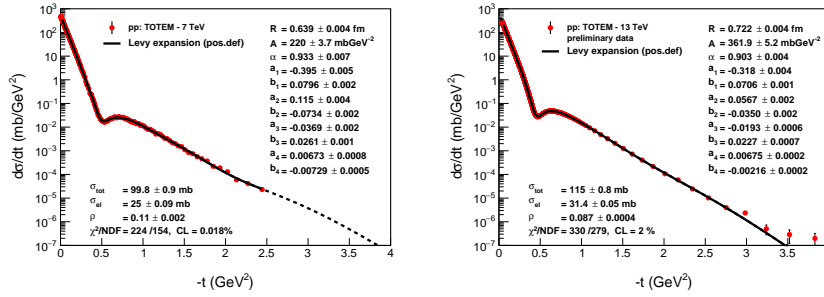


Fig. 1. Lévy series fits to elastic  $pp$  scattering data by the TOTEM Collaboration at the LHC energy of  $\sqrt{s} = 7$  TeV (left panel), and 13 TeV (right panel).

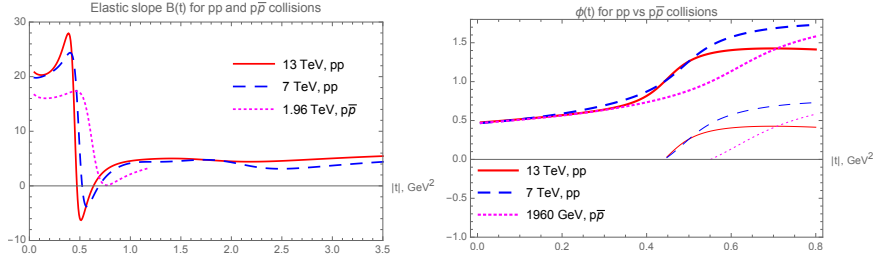


Fig. 2. The elastic slope  $B(t)$  (left panel) and the nuclear phase  $\phi(t)$  (in units of  $\pi$ , right panel) as functions of  $t$  for three distinct energies of  $pp$  and  $p\bar{p}$  collisions.

### 3.1. Characteristics of elastic scattering

One of the most important characteristics of the elastic scattering processes is the  $t$ -dependent elastic slope  $B(t)$  defined as  $B(t) \equiv d/dt (\ln d\sigma/dt)$ . One is interested in  $B = B(t = 0)$ , which requires an extrapolation of the measured differential cross-sections to the  $t = 0$  optical point. This is typically done by using an exponential approximation. As the Lévy series for

the elastic amplitude (1) is not an analytic function at  $t = 0$  for  $\alpha < 1$ , our  $B(t = 0)$  is a divergent quantity, if  $\alpha < 1$ . However,  $B(t)$  exists at the finite, measurable  $t < 0$  values, and it is this  $B(t)$  function that can be compared to the experimental determinations of  $B$ , paying also attention to the range of  $t$  where the nuclear slope parameters have been experimentally evaluated. The elastic slope function  $B(t)$  is shown for  $pp$  ( $\sqrt{s} = 7$  and 13 TeV) and  $p\bar{p}$  ( $\sqrt{s} = 1.96$  TeV) elastic scattering on the left panel of Fig. 2.

### 3.2. Odderon effects.

The  $pp$  scattering exhibits a well-defined dip-and-bump structure which results in crossings of the  $B(t)$  function through the  $B(t) = 0$  line. After the second zero-crossing,  $B(t)$  in  $pp$  reaches an extended and surprisingly flat plateau in the tail regions of large  $|t|$ . This feature is an indication of a small substructure inside the proton, with a characteristic size and cross-section that is detailed in ref. [15]. In contrast, in  $p\bar{p}$  collisions at Tevatron with  $\sqrt{s} = 1.96$  TeV, we do not observe any dip-and-bump structure, instead, one sees a shoulder-like structure. Indeed, the corresponding  $B(t)$  function does not cross zero in a statistically significant manner. Such a robust qualitative difference between the differential cross-sections of elastic  $pp$  and  $p\bar{p}$  scattering is a signature of the Odderon exchange, as detailed in refs. [13, 15]. The nuclear phase  $\phi(t)$  is defined as  $T_{el}(t) = |T_{el}(t)| \exp(i\phi(t))$ , corresponding to the right panel of Fig. 2. Thinner lines represent the principal value of  $\phi(t)$ , with  $0 \leq \phi_{PV} < \pi$ . Fig. 2 shows that  $\phi(t)$  reaches the value of  $\pi$  at the same value of  $|t|$  in  $pp$  collisions both at  $\sqrt{s} = 7$  and at 13 TeV, but at a different value in  $p\bar{p}$  collisions at  $\sqrt{s} = 1.96$  TeV, proposed as a second signature of the Odderon [13].

### 3.3. (Sub)structure(s) of the proton from elastic scattering

The summary plots of the zeroth-order  $d\sigma/dt = A \exp(-(R^2|t|)^\alpha)$  Lévy fits are shown on Fig. 3. The left and right panels indicate the leading order shape of the diffractive cone at low- $t$ , as well as the tail or large  $-t$  regions, respectively. Both regions are well described with an  $\alpha = 0.9$  fixed value. The overall size of the protons is increasing with increasing colliding energies, as evidenced by the steepening of the zeroth order Lévy fits on the left panel of Fig. 3. However, the tail fits on the right panel of Fig. 3 show parallel lines at the ISR energies, indicating a sub-structure with nearly unchanged size in the  $\sqrt{s} = 23.5 - 62.5$  GeV energy range. At the LHC energy range of  $\sqrt{s} = 7 - 13$  TeV, the tail fits again show two lines that are parallel to one another, indicating a sub-structure at LHC energies, too. However, these lines are not parallel with but significantly steeper as compared to the fits to the tail of the ISR datasets. In ref. [13], these results were in-

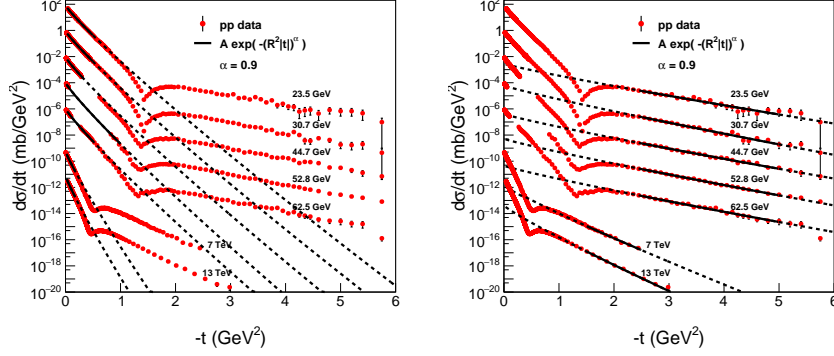


Fig. 3. Summary plots of the zeroth-order Lévy fits,  $d\sigma/dt = A \exp(-R^2|t|^\alpha)$ , to the diffractive cone (left panel) and to the tail (right panel) regions of the elastic  $pp$  scattering data from  $\sqrt{s} = 23.4$  GeV to 13 TeV, with  $\alpha = 0.9$  fixed.

terpreted in terms of proton substructure(s). At the lower ISR energies, a smaller substructure with a nearly energy independent size is evidenced by the slope  $B_{\text{tail}}(pp|ISR) \approx 2 \text{ GeV}^{-2}$ . At the LHC energies of  $\sqrt{s} = 7$  and 13 TeV, the slope at large  $-t$  changes dramatically to  $B_{\text{tail}}(pp|LHC) \approx 5 \text{ GeV}^2$ , indicating a larger sub-structure of the protons at these energies.

### 3.4. Proton profiles

Let us switch to the impact parameter space as

$$t_{el}(b) = \int \frac{d^2\Delta}{(2\pi)^2} e^{-i\Delta\mathbf{b}} T_{el}(\Delta) = i \left[ 1 - e^{-\Omega(b)} \right], \quad \Delta \equiv |\Delta|, \quad b \equiv |\mathbf{b}|.$$

The opacity  $\Omega(b)$  is a complex function that defines the shadow profile as

$$P(b) = 1 - \left| e^{-\Omega(b)} \right|^2 = [2 - \text{Im} t_{el}(b)] \text{Im} t_{el}(b) - [\text{Re} t_{el}(b)]^2. \quad (2)$$

Fig. 4 indicates the shadow profile of protons at  $\sqrt{s} = 7$  and 13 TeV in  $pp$  and at  $\sqrt{s} = 1.96$  TeV in  $p\bar{p}$  collisions. A nearly black region opens up in the TeV energy region, where  $P(b) \approx 1$ . This region increases with increasing colliding energies, and it is surrounded by a gray “hair” or “skin” region, where  $P(b)$  drops from its maximum to zero with nearly the same decrease at all energies. At very large colliding energies, the protons do become blacker and larger, but they do not become edgier, confirming ref. [19].

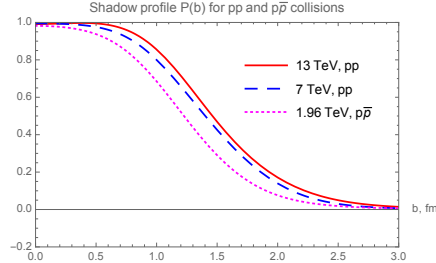


Fig. 4. The shadow profile  $P(b)$  for three distinct energies of  $pp$  and  $p\bar{p}$  collisions.

#### 4. Outlook

Interesting further details about the theory of imaging, as applied to the internal structure of the protons at LHC energies by elastic scattering, were summarized and highlighted recently in refs. [15, 20, 21].

#### REFERENCES

- [1] G. Antchev *et al.* [TOTEM Collaboration], arXiv:1712.06153 [hep-ex].
- [2] G. Antchev *et al.* [TOTEM Collaboration], arXiv:1812.04732 [hep-ex].
- [3] L. Lukaszuk and B. Nicolescu, *Lett. Nuovo Cim.* **8**, 405 (1973).
- [4] A. P. Samokhin and V. A. Petrov, *Nucl. Phys. A* **974**, 45 (2018).
- [5] V. A. Khoze, A. D. Martin, M. G. Ryskin, *Phys. Rev. D* **97**, 034019 (2018).
- [6] V. A. Khoze, A. D. Martin and M. G. Ryskin, *Phys. Lett. B* **780**, 352 (2018).
- [7] Y. M. Shabelski and A. G. Shuvaev, *Eur. Phys. J. C* **78**, no. 6, 497 (2018).
- [8] M. Broilo, E. G. S. Luna and M. J. Menon, arXiv:1803.06560 [hep-ph].
- [9] M. Broilo, E. G. S. Luna and M. J. Menon, *Phys. Lett. B* **781**, 616 (2018).
- [10] E. Martynov and B. Nicolescu, arXiv:1804.10139 [hep-ph].
- [11] S. M. Troshin and N. E. Tyurin, arXiv:1805.05161 [hep-ph].
- [12] I. M. Dremin, *Universe* **4**, no. 5, 65 (2018).
- [13] T. Csörgő, R. Pasechnik and A. Ster, arXiv:1807.02897 [hep-ph].
- [14] G. Antchev *et al.* [TOTEM Collaboration], arXiv:1812.08283 [hep-ex].
- [15] T. Csörgő, R. Pasechnik and A. Ster, arXiv:1811.08913 [hep-ph].
- [16] T. Csörgő and S. Hegyi, *Phys. Lett. B* **489** (2000) 15.
- [17] M. B. De Kock, H. C. Eggers and T. Csörgő, *PoS WPCF* **2011** (2011) 033.
- [18] G. Antchev *et al.* [TOTEM Collaboration], *Nucl. Phys. B* **899**, 527 (2015).
- [19] F. Nemes, T. Csörgő, M. Csanád, *Int. J. Mod. Phys. A* **30**, 14, 1550076 (2015)
- [20] V. P. Goncalves and P. V. R. G. Silva, arXiv:1811.12250 [hep-ph].
- [21] I. M. Dremin, *Particles* **2**, no. 1, 57 (2019).